ACS APPLIED MATERIALS & INTERFACES

Research Article

www.acsami.org

Semicrystalline Structure–Dielectric Property Relationship and Electrical Conduction in a Biaxially Oriented Poly(vinylidene fluoride) Film under High Electric Fields and High Temperatures

Lianyun Yang,[†] Janet Ho,[‡] Elshad Allahyarov,[†,∥,§] Richard Mu,[⊥] and Lei Zhu*[,†]

[†]Department of Macromolecular Science and Engineering, Case Western Reserve University, Cleveland, Ohio 44106-7202, United States

[‡]Army Research Laboratory, RDRL-SED-C, 2800 Powder Mill Road, Adelphi, Maryland 20783, United States

[§]Theoretical Department, Joint Institute for High Temperatures, Russian Academy of Sciences, Izhorskaya 13/19, 117419 Moscow, Russia

[∥]Institut für Theoretische Physik, Heinrich-Heine-Universität Düsseldorf, D-40225 Düsseldorf, Germany

[⊥]Department of Physical and Life Sciences, Fisk University, Nashville, Tennessee 37208, United States

Supporting Information

ABSTRACT: Poly(vinylidene fluoride) (PVDF)-based homopolymers and copolymers are attractive for a broad range of electroactive applications because of their high dielectric constants. Especially, biaxially oriented PVDF (BOPVDF) films exhibit a DC breakdown strength as high as that for biaxially oriented polypropylene films. In this work, we revealed the molecular origin of the high dielectric constant via study of a commercial BOPVDF film. By determination of the dielectric constant for the amorphous phase in BOPVDF, a high value of ca. 21–22 at 25 °C was obtained, and a three-phase (i.e., lamellar crystal/oriented interphase/amorphous region) semicrystalline model was proposed to explain this result. Meanwhile, electronic conduction mechanisms in BOPVDF under high electric fields and elevated temperatures were investigated by thermally stimulated depolarization current (TSDC) spectroscopy and leakage current studies. Space charge injection from metal electrodes was identified as a major factor for electronic conduction when BOPVDF was poled above 75 °C and 20 MV/m. In addition, when silver or aluminum were used as electrodes, new ions were generated from electrochemical reactions under high fields. Due to the electrochemical reactions between PVDF and the metal electrode, a question is raised for practical electrical applications using PVDF and its copolymers under high-field and high-temperature conditions. A potential method to prevent electrochemical degradation of PVDF is proposed in this study.

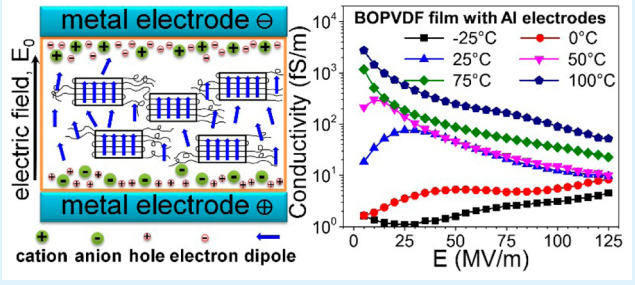

KEYWORDS: *poly(vinylidene fluoride), dielectric constant, electronic conduction, thermally stimulated depolarization current, space charge injection, ionic polarization*

1. INTRODUCTION

Biaxially oriented polypropylene (BOPP) has been the state-of-the-art dielectric polymer for film capacitors,[1,2] which find many practical applications such as power electronics in electric drive vehicles,[3,4] pulsed power,[5,6] and medical devices (e.g., defibrillators).[7] This is because of its high breakdown strength, low dielectric loss, and long dielectric life.[8,9] However, the dielectric constant for BOPP is only 2.25, and thus, its energy density is low, resulting in larger sizes and higher costs as compared to electrolytic capacitors.[10] To miniaturize polymer film capacitors and lower its cost, high dielectric constant polar polymers have become increasingly attractive.[11−14] The challenge for polar dielectric polymers lies in how to avoid or minimize high dielectric losses. For example, poly(vinylidene fluoride) (PVDF) has a much higher dielectric constant (10–12 at 1 kHz at 25 °C) than BOPP, and its thermal properties are comparable to those of BOPP. In addition, it can also be tenter-line processed into high quality thin (3–10 μm) films (i.e., biaxially oriented PVDF (BOPVDF)). Under a DC voltage, BOPVDF exhibited a similar breakdown strength as that of BOPP, i.e., 720–770 MV/m.[15] Therefore, BOPVDF films seem to be attractive for film capacitor applications.

However, PVDF is a well-known ferroelectric polymer,[16,17] and thus, BOPVDF cannot be used for film capacitors under AC conditions because of its significant hysteresis in (crystalline) dipole switching above the coercive field (E_c, ca. 70 MV/m for the β phase[18]). Therefore, substantial research efforts have been dedicated to reducing the ferroelectric

Received: April 5, 2015
Accepted: June 29, 2015
Published: June 29, 2015

DOI: 10.1021/acsami.5b02944
ACS Appl. Mater. Interfaces 2015, 7, 19894–19905

hysteresis using PVDF random copolymers and terpolymers.[11−14] For example, P(VDF-*co*-trifluoroethylene) [P(VDF-TrFE)]-based copolymers (electron beam or γ ray-irradiated) and terpolymers have shown narrow hysteresis loops due to crystal pinning and nanodomain formation as a result of crystal isomorphism (i.e., defect-modified crystals).[13,14] Nonetheless, the low Curie point (around room temperature), low melting temperature (ca. 120 °C), and extremely high cost (>$5,000/kg) have prevented broad and large-scale applications of P(VDF-TrFE)-based copolymers and terpolymers. On the other hand, the switching of crystalline dipoles in ferroelectric PVDF can be suppressed under continuous DC poling conditions.[19] Therefore, BOPVDF may be useful for DC applications because its dielectric constant under DC conditions is still as high as 10−12. In this study, we intend to explain the origin of high dielectric constant for BOPVDF based on its oriented crystalline and amorphous structures. Meanwhile, the electronic DC conductivity of the BOPVDF film is investigated under high electric fields, high temperatures, and long-time poling conditions using the leakage current study. The mechanisms of dipolar polarization, charge injection from metal electrodes, and polarization of ions are studied by thermally stimulated depolarization current (TSDC) spectroscopy. In the following, we will briefly introduce various polarization processes, such as dipolar polarization, charge injection, and ionic polarization, in a BOPVDF film under a sufficiently high DC field.

Scheme 1 shows various types of polarization events in an oriented PVDF film under a sufficiently high DC poling electric field. First, amorphous and crystalline PVDF dipoles will orient fairly quickly along the electric field direction. Second, homocharges (i.e., the same sign as the corresponding electrode) such as electrons and holes will be injected from the metal electrodes into the film and accumulate near the film-electrode interfaces.[20] Third, PVDF usually contains subppm levels of impurity ions[21,22] due to the suspension polymerization method used in industry.[23] Under a DC electric field, ionic species can be polarized toward oppositely charged electrodes, forming an electric double layer at the sample-metal electrode interface.[24] These ionic charges are heterocharges because they have an opposite sign as the compensating metal electrode.[20] As shown in Scheme 1, polarized dipoles and heterocharges will create an opposite internal electric field in the PVDF film. It is expected that they tend to decrease the local electric field and thus decrease the electronic conduction in the polar polymer film. Injected homocharges will create a parallel internal electric field along the applied field. Therefore, it is expected that they tend to increase the local field and thus increase the electronic conduction. In this study, we will address the following questions: What are the effects of these polarization events under various poling conditions (i.e., different electric fields, temperatures, and times)? Which is the most important factor for the electrical conduction in a polar polymer film?

Scheme 1. Schematic Representation for Polarized Amorphous and Crystalline Dipoles, Injected Homocharges, and Polarized Ionic Species (i.e., Heterocharges) for an Oriented PVDF Film under a Sufficiently High DC Electric Field

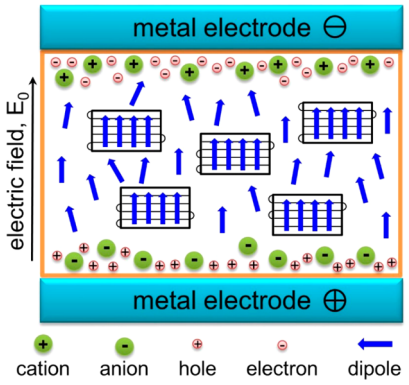

2. RESULTS AND DISCUSSION

2.1. Oriented Crystalline Structure in the BOPVDF Film. The crystalline structure of the BOPVDF film was characterized by WAXD and FTIR, respectively (Figure 1A,B). The 1D WAXD profile at 25 °C was obtained by integrating the corresponding 2D pattern (see the inset of Figure 1A). All major reflections for the α and β crystals were assigned accordingly.[25,26] As a result of biaxial stretching, the mixed $(021/111)_\alpha$ reflections did not show specific orientation when the X-ray beam was directed parallel to the film normal. However, the $(020)_\alpha$, $(110)_\alpha$, $(201)_\alpha$ and $(002)_\alpha$ reflections showed a preferred orientation with the α crystal *c* axes in the horizontal direction. Meanwhile, sharp $(110/200)_\beta$ and $(001)_\beta$ reflections showed a clear orientation with the β crystal *c*-axes in the vertical direction. The Herman's orientation factor (f_H) for the $(110)_\alpha$ and $(110/200)_\beta$ reflections were calculated to compare the degree of orientation for the α and β phases; f_H = 0.43 for $(110)_\alpha$ and f_H = 0.57 for $(110/200)_\beta$. Apparently, the higher orientation factor for the $(110/200)_\beta$ reflection indicated that the β phase had a better degree of orientation than the α phase. We speculate that in the tenter-line processing, the machine direction in the first step stretching should be along the horizontal direction to orient the α crystals (which was crystallized from the stretched melt), whereas the transverse direction in the second stretching step should be along the vertical direction to induce some β crystals (which was formed by stretching the α crystals). Note that in the tenter-line processing, the film is stretched first in machine (or extrusion) direction, followed by subsequent stretching using tenter clips along the transverse direction.[27]

Due to the lack of absolute X-ray diffraction intensities for the α and β phases, WAXD was not used to determine the relative contents of the α and β crystals in the BOPVDF film. Instead, they were determined by FTIR in the transmission mode. From Figure 1B, absorption bands at 489, 531, 615, 764, 795, and 1215 cm^{-1} were assigned to the α phase and those at 468, 511, 841, and 1280 cm^{-1} were assigned to the β phase.[28] The relative content of the β phase [F(β)] was calculated by $F(\beta) = A_\beta/(1.3A_\alpha + A_\beta)$, where A_α and A_β are the absorbance (i.e., integrated peak areas from peak-fitting) at 764 and 841 cm^{-1}, respectively.[29,30] From Figure 1B, the relative content of β crystals was only ca. 0.30, suggesting that the α phase was the major crystalline phase for the BOPVDF film. In addition, the electrically poled sample was also studied by FTIR. After the short-circuit electric poling, the intensities of the absorption bands for the α phase at 489 and 1215 cm^{-1} decreased as compared to those for the fresh film, suggesting certain conversion of the α phase into the β phase induced by the poling field of 200 MV/m at room temperature for 3 h. Meanwhile, the intensities of the absorption bands for the β

DOI: 10.1021/acsami.5b02944
ACS Appl. Mater. Interfaces 2015, 7, 19894−19905

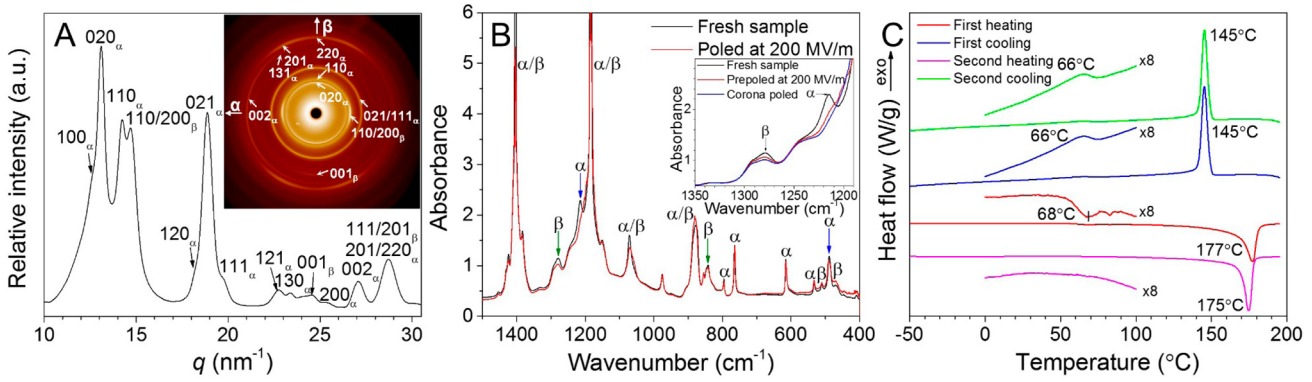

Figure 1. (A) 1D WAXD profile and corresponding 2D pattern for the BOPVDF film at 25 °C. Major reflections for the α and β phases are assigned. (B) FTIR spectra for the fresh and electrically prepoled (200 MV/m for 3 h at room temperature) BOPVDF films. (Inset) Magnified region between 1200 and 1350 cm^{-1}. (C) DSC first heating, first cooling, second heating, and second cooling curves for the BOPVDF film. The heating and cooling rates are 10 °C/min. Temperature ranges from 0 to 100 °C are magnified 8 times for clarity.

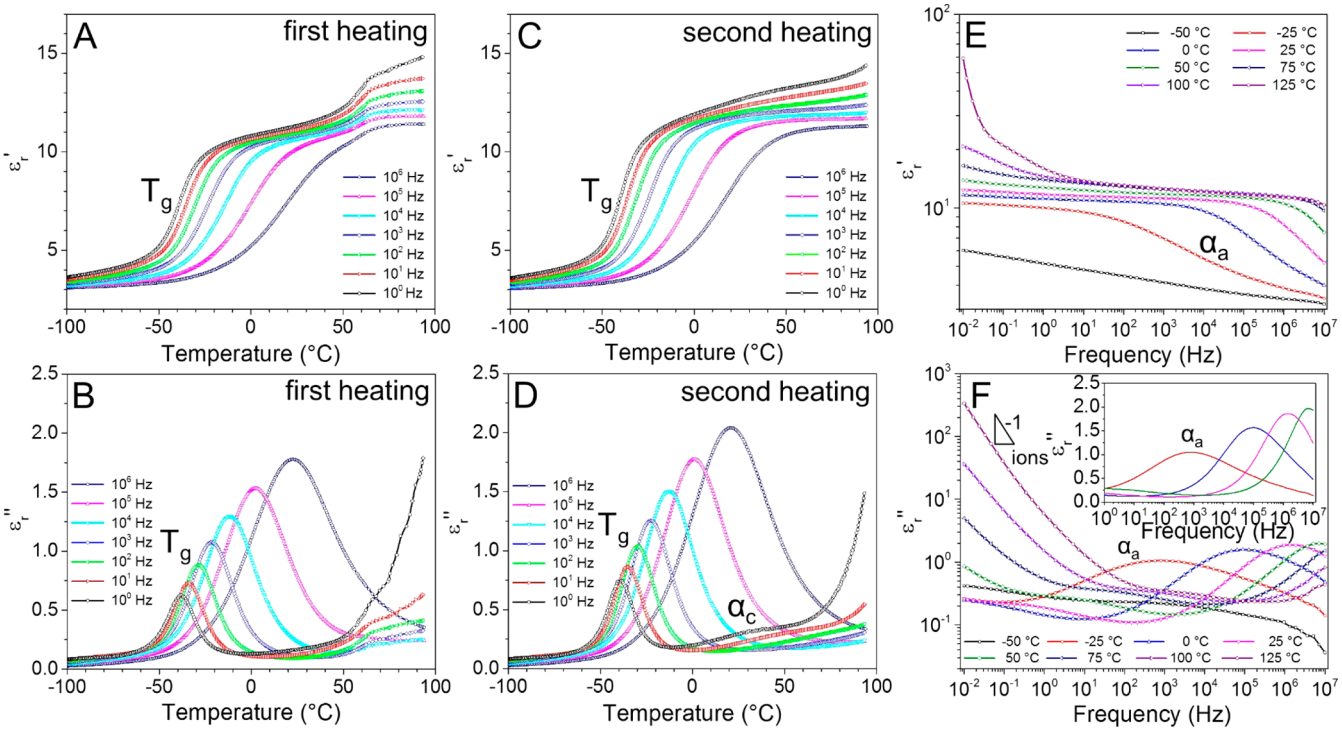

Figure 2. (A and C) Real (ε_r') and (B and D) imaginary (ε_r'') parts of relative permittivity as a function of temperature at different frequencies during the first and second heating process for the biaxially stretched PVDF film. (E) ε_r' and (F) ε_r'' as a function of frequency at different temperatures for the same PVDF film. (F, inset) Linear scale plot for the ε_r'' between −25 and 50 °C.

phase at 841 and 1280 cm^{-1} also decreased. This could be explained by the electric field-induced alignment of the $-CH_2CF_2-$ (or VDF) dipoles in the β crystals. Note that major contributions to the IR absorption bands at 841 and 1280 cm^{-1} are attributed to the symmetric and asymmetric stretching modes of CF_2 groups in the β crystal.[28] These modes will have a maximum IR absorption when the β dipoles are oriented perpendicular to the film normal (i.e., lying in the film). On the contrary, they will have a minimum IR absorption when the β dipoles are oriented parallel to the film normal. For the nonpoled fresh sample, the β dipoles were randomly oriented and should show some IR absorption. After electric poling, a certain amount of β dipoles remained oriented along the film normal (i.e., the electric field) direction. Consequently, the IR absorption would decrease. Note that the FTIR result for the electrically poled film was obtained about 1 week after the electrical poling at room temperature. The amorphous dipoles had a fast relaxation at room temperature (~1 μs; see frequency-scan BDS results in Figure 2E,F) and thus should have already relaxed after 1 week of aging at room temperature. The orientation effect in FTIR should arise solely from the β dipoles in the crystals. It was reported that electrically aligned β dipoles in the PVDF film will not relax until the temperature reached above 80 °C.[31,32]

The degree of β crystalline dipole alignment in the electrically poled film is compared to a corona-poled film, as shown in the inset of Figure 1B. The corona poling was performed at room temperature with a needle voltage of 20 kV and a grid voltage of 5 kV for 5 min. From the literature report,[33] this corona poling condition should be sufficient to

DOI: 10.1021/acsami.5b02944
ACS Appl. Mater. Interfaces 2015, 7, 19894−19905

maximize the β dipole orientation in PVDF films. After corona poling, the intensities of the absorption bands at 1215 cm^{-1} for the α phase and at 1280 cm^{-1} for the β phase further decreased, as compared to those for the electrically poled film. Obviously, corona poling was more effective in transforming the α phase into the β phase, as well as aligning the β dipoles along the field direction. From this comparison, we calculated that the electric poling at 200 MV/m for 3 h was about 56% as effective as the corona poling in aligning the β dipoles. We did not choose a longer poling time because the film breakdown strength would decrease at longer poling times. Although the corona-poled film had a higher degree of β dipole orientation, we could not use it for later TSDC and leakage current studies, because corona poling also introduced conductive charge carriers (i.e., electrons and plasma ions) into the BOPVDF film.[34] As a result, the electronic conductivity increased and the breakdown strength significantly decreased as compared to the fresh and electrically poled BOPVDF films.

Thermal property of the BOPVDF film was characterized by DSC, and results are shown in Figure 1C. Temperature ranges between 0 and 100 °C were magnified 8 times for clarity. During the first heating, a weak crystal melting peak was observed around 68.4 °C before the major melting peak at 177 °C. Upon the first (as well as the second) cooling from the melt, a secondary crystallization peak was observed at 66 °C in addition to the primary crystallization peak at 145 °C. Note that secondary crystallization mostly refers to additional crystallization of the amorphous region (mostly tie and dangling molecules) in between existing primary crystalline lamellae.[35] Judging from the crystallization temperature of 66 °C, the secondary crystallization should be homogeneously nucleated, because homogeneously nucleated nonisothermal crystallization for PVDF has been reported around 55−70 °C in nanoconfined droplets.[36,37] Upon the second heating, no trace of this melting peak as in the first heating was observed between 0 and 100 °C, suggesting that the melting point for the newly formed secondary crystals during cooling from the melt should be at least above 90 °C (Figure 1C). This was understandable, considering a finite supercooling for the newly secondary crystals. On the basis of this experimental result, the weak melting peak at 68.4 °C during the first heating should be attribute to the melting of poor secondary crystallites formed during biaxially orientation. After melt-recrystallization, these poor secondary crystallites would not form again. Instead, during the second heating, a broad premelting process showed an onset around 80 °C before the major melting peak at 175 °C. Assuming the heat of fusion for the perfect PVDF crystal is 104.6 J/g,[38] the weight fraction crystallinity for the BOPVDF film during the first heating was $x_{c,w}$ = 54 wt %. The reason for the broad premelting of the secondary crystallites and relatively low crystallinity could be attributed to the existence of about 3−6 mol % head-to-head and tail-to-tail (HHTT) defects in PVDF homopolymers.[25]

2.2. Enhanced Dielectric Property Due to Oriented Amorphous Interphases. The dynamic dielectric properties of the BOPVDF film were studied by both temperature- and frequency-scan BDS. Figure 2A,B shows the real (ε_r') and the imaginary (ε_r'') parts of the relative permittivity during the first heating (up to 100 °C), and Figure 2C,D show the ε_r' and ε_r'' during the second heating. From both heating results (Figure 2B,D), the glass transition temperature (T_g) of the BOPVDF film was identified as the relaxation peak at −39 °C and 1 Hz, and it gradually increased to higher temperatures upon increasing frequency. Below the glass transition, the ε_r' value was only about 3.1 at −100 °C and 10^6 Hz (Figure 2A,C). Above the T_g (e.g., > 0 °C), the ε_r' value increased to above 10. Note that the applied electric field in BDS measurements was only 0.125 MV_{rms}/m, much lower than the typical coercive field (E_c) for the β PVDF crystals (i.e., $E_c \sim 70$ MV/m).[18] At the same time, the α and β chain axes in the crystals were well-oriented parallel to the film due to biaxial orientation. Therefore, this increase of the ε_r' from 3.1 at −100 °C to >10 above the T_g indicated that the relatively high dielectric constant for BOPVDF in Figure 2A was a result of polarization of the amorphous dipoles, rather than the crystalline dipoles. If we assume that the contribution of crystalline dipoles to the dipolar polarization is negligible for the well-oriented PVDF film at low electric fields, we shall be able to extract the dielectric constant for the amorphous phase.

Taking into account of the crystallinity of 54 wt % and the dielectric constant at 0.01 Hz and 25 °C is about 12.4, we can estimate the static dielectric constant, ε_{rs}^a, for the amorphous phase as high as ca. 21−22 (for detailed calculation, see section 2 in the Supporting Information). This value is significantly higher than both experimental (8−13) and computer simulation values (9.7 at 300 K and 12.5 at 400 K).[39] In previous reports, an interphase was proposed at the amorphous−crystal boundaries:[40] Due to the existence of the HHTT structural defects, a certain amount of PVDF chains stemmed out of the crystal basal plane, rather than forming reentrant folds (i.e., the adjacent reentry model). As shown in Scheme 2, the amorphous chains in the interphase regions orient more or less parallel to the stretching direction because of the perfect alignment of the crystals. This orientation is ideal for electrical polarization because the main-chain VDF dipoles can be more easily rotated by the electric field than those in randomly oriented chains. In the past, it has been reported that

Scheme 2. Schematic Representation for the BOPVDF Film Containing Oriented Primary and Secondary Crystals, Bulk Amorphous Phase with a Random Orientation, And Oriented Amorphous Interphase Regions (Highlighted in Blue) Under an Alternating External Field[a]

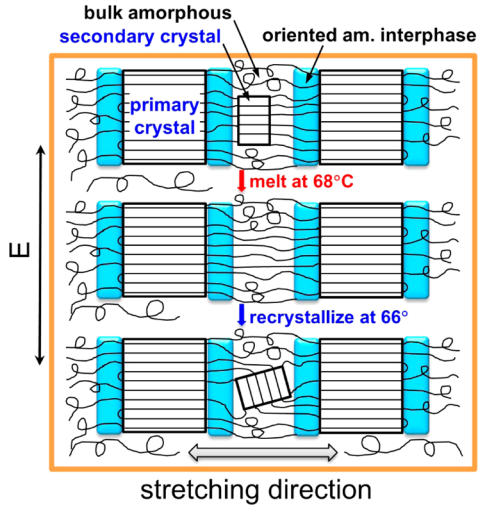

[a](Top) Fresh BOPVDF with a parallel-aligned secondary crystal. (Middle) After melting of the secondary crystals during the first heating. (Bottom) After recrystallization of a new secondary crystal with a more or less random orientation.

DOI: 10.1021/acsami.5b02944
ACS Appl. Mater. Interfaces 2015, 7, 19894−19905

crystal orientation has an anisotropic effect on the dielectric constant for PVDF and its random copolymer films.[41,42] For example, the dielectric constant appears higher (~10−12) for films with crystal/chain axes perpendicular to the film normal direction than that (~5−6) for films with crystal axes parallel to the film normal direction. This was explained by different orientations and responses of crystalline dipoles in the BOPVDF films. Actually, this explanation is incorrect. As we mentioned above, the contribution from crystalline dipoles to the dipolar polarization should be negligible at low electric fields when the chains are oriented perpendicular to the film normal. Instead, it is the orientation of the interfacial amorphous PVDF chains that increases the ε_{rs}^{a} for the amorphous PVDF and thus the overall dielectric constant of oriented PVDF films.

In section 3 of the Supporting Information, we estimate the fraction (f) of the interphase regions in the amorphous PVDF phase. Using the static dielectric constant estimated for the amorphous PVDF in the BOPVDF film (i.e., ε_{rs}^{a} = 21.6), the fraction is calculated to be 0.55. This means that nearly 55% of the amorphous phase in the BOPVDF film is the interphases with homeotropic amorphous chains on the crystal basal plane. We consider that this physical picture of crystalline lamellae, liquid crystalline-like interphases, and bulk amorphous region should be general for those semicrystalline polymers, which have a significant amount of chains stemming out from the crystal basal surface (i.e., the switchboard model), rather than the adjacent reentry.[43] Nevertheless, the above calculations are rough estimations. In the future, more research needs to be carried out to experimentally understand the adjacent reentry versus switchboard models, and quantitatively determine the fraction of the interphase regions in the amorphous phase of semicrystalline PVDF (and its random copolymers).

In Figure 2A, another stepwise increase in the ε_r' was observed around 60 °C for the first heating at nearly all frequencies except for 10^6 Hz, where the glass transition merged with this step increase. For example, at 1 Hz, the ε_r' increased from 11.6 at 35 °C to 14.1 at 75 °C. This step increase in ε_r' during the first heating could be attribute to the melting of the poor secondary crystallites formed during biaxial stretching (see the weak melting peak at 68 °C in the magnified first heating DSC curve in Figure 1C), because it did not show up during the second heating in Figure 2C. Instead, a weak α_c relaxation peak was observed around 30 °C during the second heating in the ε_r'' plot in Figure 2D, whereas this α_c relaxation peak was absent before 50 °C for the first heating in Figure 2B. Here, the α_c relaxation refers to the switching of slightly tilted CF_2 dipoles along the chain axes in the α crystal under an alternating electric field.[42,44] In the fresh BOPVDF film, poor secondary α crystallites were formed during stretching, and their chain axes must orient parallel to the film (top panel, Scheme 2). Consequently, no α_c relaxation should be seen during the first heating below their melting starting at 50 °C. After these secondary crystals melted, the molten chains might still keep certain orientation (middle panel, Scheme 2). Although the melting enthalpy was only about 5.4% of the total crystallinity (DSC result, Figure 1C), these oriented amorphous chains substantially increased the dielectric constant from 11.6 at 35 °C to 14.1 at 75 °C at 1 Hz. After recrystallization (i.e., heating to 100 °C in the first heating and then cooling to −100 °C), secondary crystallization happened (weak exothermic peak at 66 °C in the cooling DSC curves, Figure 1C) with more or less randomly oriented secondary α crystallites (bottom panel, Scheme 2). Consequently, a weak α_c relaxation peak (e.g., around 30 °C at 1 Hz) was observed before the onset (80 °C) of premelting shoulder during the second heating (Figure 2D). Because of this weak α_c relaxation during the second heating, the ε_r' showed a broad and gradual increase between 0 and 75 °C in Figure 2C (e.g., 11.9 at 0 °C to 13.7 at 75 °C at 1 Hz).[42] During both the first and second heating processes (Figure 2B,D), significant loss with additional increase in ε_r' (Figure 2A,C) was observed above 80 °C, especially at 1 Hz. This could be attributed to the continued premelting of the poor PVDF crystallites.

Figure 2E,F shows frequency-scan results for the fresh BOPVDF film at temperatures ranging from −50 to 125 °C. Slightly below the T_g (e.g., at −50 °C), the ε_r' gradually decreased from 6.0 at 10^{-2} Hz to 3.1 at 10^7 Hz due to the fact that most amorphous dipoles were still frozen. Above the T_g at −39 °C and below 75 °C, a broad α_a relaxation due to amorphous dipoles in both bulk amorphous and interphase regions was clearly seen at each temperature in Figure 2E,F. With increasing temperature, the plateau dielectric constant at low frequencies (i.e., $\varepsilon_{rs,film}'$) gradually increased (Figure 2E). Meanwhile, the breadth of the α_a relaxation peak gradually decreased and its intensity gradually increased (linear-scale plot, inset of Figure 2F). This behavior cannot be explained by the classic Debye theory on a dipolar relaxation process with a single relaxation time, that is, Debye dispersion equation:[45]

$$\varepsilon_r^* = \varepsilon_{r\infty} + \frac{\varepsilon_{rs} - \varepsilon_{r\infty}}{1 + i\omega t} \tag{1}$$

where ε_r^* is the complex dielectric constant of the BOPVDF film, ω is the angular frequency, and t is time. At the relaxation peak, we have

$$\varepsilon_r', \text{ max} = (\varepsilon_{rs} + \varepsilon_{r\infty})/2 \tag{2}$$

and

$$\varepsilon_{r,max}'' = (\varepsilon_{rs} - \varepsilon_{r\infty})/2 \tag{3}$$

These values, as well as the breadth of the relaxation peak, should not change much with varying temperature. Note that in cases with relatively weak dipolar interactions,[46] the $\varepsilon_{r,max}''$ should decrease with increasing temperature because the dipolar polarizability usually decreases with increasing temperature (eqs S1 and S16, Supporting Information). On the basis of the experimental observations in Figure 2E,F, we consider that there must exist a distribution of relaxation times for the bulk amorphous region and the interphases. This is similar to the case of the rigid amorphous phase observed in semicrystalline polymers,[47] where the rigid amorphous phase is more rigid and thus has slower dynamics than the bulk amorphous phase near the T_g. At low temperatures, the distribution of the relaxation times for both bulk amorphous region and the interphases is broad, resulting in a broader relaxation peak. Upon increasing temperature, the distribution becomes narrower, resulting in narrower relaxation peaks at high temperatures. Meanwhile, increases in $\varepsilon_{rs,film}'$ (Figure 2E) and $\varepsilon_{r,film,max}''$ (inset of Figure 2F) with temperature can be qualitatively explained by the Kirkwood−Fröhlich theory in eq S16 (Supporting Information). At low temperatures, the rigid fraction is dominant (i.e., $N_{dip,a}$ is low), the interaction among dipoles is weak, or both. As a result, the ε_{rs} becomes low, and thus, $\varepsilon_{rs,film}'$ and $\varepsilon_{r,film,max}''$ are low, as deduced from eq S16 (Supporting Information) and eq 3. Upon increasing temperature, the rigid interphases become more mobile (i.e.,

DOI: 10.1021/acsami.5b02944
ACS Appl. Mater. Interfaces 2015, 7, 19894−19905

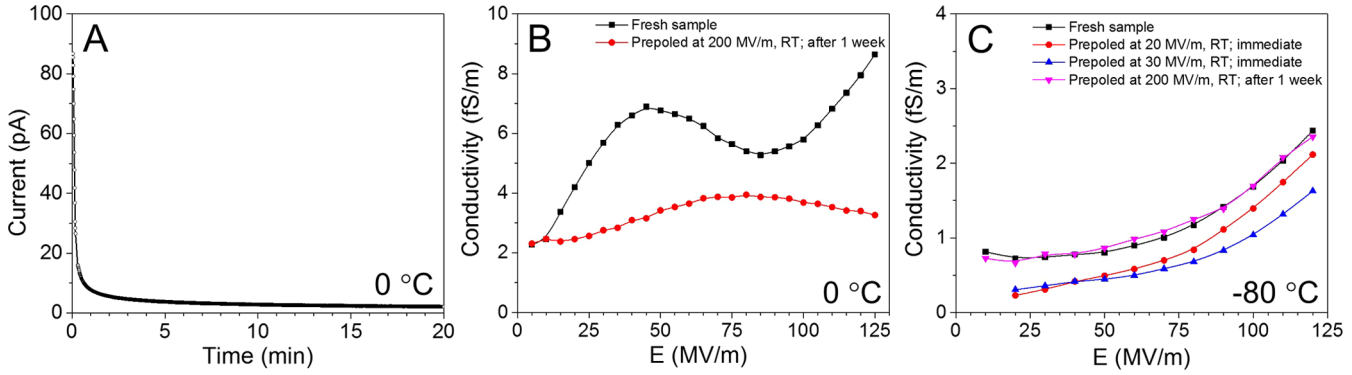

Figure 3. (A) Leakage current for the fresh BOPVDF film under a poling field of 50 MV/m at 0 °C during a stepwise poling process (starting at 5 MV/m with increment of 5 MV/m). (B) DC conductivity at 0 °C for fresh and 200 MV/m-poled BOPVDF films. (C) DC conductivity at −80 °C for the fresh and various electrically poled BOPVDF films: the first sample is the 200 MV/m-poled film, and the second and third samples are in situ poled samples at 20 and 30 MV/m at room temperature for 20 min, respectively.

$N_{dip,a}$ increases), the interactions among dipoles (especially for the interphases) become stronger, or both. Therefore, the ε_{rs} increases, and thus, both $\varepsilon'_{rs,film}$ and $\varepsilon''_{r,film,max}$ increase. This is also observed in the molecular dynamics simulation result:[39] ε^{a}_{rs} = 12.5 at 400 K. Using eq S16 (Supporting Information), the correlation parameter for the randomly oriented PVDF melt, g_{3D}, is calculated to be 6.53 for μ_a = 0.932 D (assuming the interphase fraction f is zero), higher than that at 300 K (g_{3D} = 3.61). The increase of the intensity for the amorphous relaxation peak with frequency in the temperature-scan results (Figure 2B,D) can be explained similarly, because the relaxation peak will appear at higher temperatures with increasing frequency.

At temperatures above 75 °C, further increases were observe at the low frequency range for ε_r' and ε_r'' in Figure 2E,F. The slope in the ε_r'' at low frequencies was close to −1, especially at 125 °C, indicating the existence of impurity ions.[48] Note that values of ε_r' and ε_r'' under low frequencies and at high temperatures were significantly lower than other commercial PVDF and PVDF copolymer samples.[14,21,49] This suggested that the concentration of impurity ions and their diffusion coefficient in this BOPVDF film should be fairly low.

2.3. Different Factors Affecting Electronic Conduction in the BOPVDF Film. As we discussed in Scheme 1, electronic conduction in the BOPVDF film under high electric fields and high temperatures should be closely related to the orientation of amorphous/crystalline dipoles, ionic polarization, and injected charges. To determine pure electronic conductivity at a constant temperature, we measured the leakage current[9] while holding the sample under each electric field for 20 min, and the electric field was stepwise increased until 125 MV/m (the limit of the instrument, i.e., 1000 V_{DC}). An example of the charge current as a function of time is shown in Figure 3A for the fresh BOPVDF film at 50 MV/m and 0 °C during the stepwise poling process. In the beginning, the charge current decreased rapidly with time. Supposedly, this charging process should be fairly fast for a pure and surface defect-free dielectric material, for example, less than 1 s. Nonetheless, the charge current continuously decreased, even after 5 min. This could be attributed to ionic polarization in the sample (and surface defects) near the electrode−sample interfaces in addition to the electronic conduction (leakage) through the sample.[20] After 15 min, the charge current tended to reach a plateau value and we took the leakage current at 20 min as the DC conduction current to calculate the electronic conductivity. We did not test for longer than 30 min because the film tended to break down more readily if we used a longer holding time at each poling electric field.

First, we studied the effect of oriented crystalline dipoles on electronic conduction in the BOPVDF film at 0 °C. To avoid interference from polarization of impurity ions, we studied the leakage current of the 200 MV/m-poled BOPVDF film 1 week after the poling process. In this way, any polarized impurity ions would have relaxed. From the FTIR result in Figure 1B, some β dipoles were still aligned in the β crystals of the 200 MV/m-poled sample. Figure 3B compares the DC conductivity as a function of the electric field at 0 °C for the fresh and prepoled samples. We chose 0 °C because the mobility of impurity ions was fairly slow around and below room temperature.[50] From Figure 3B, the conductivity of the prepoled sample was slightly lower than that of the fresh sample. Therefore, we consider that the polarized β dipoles would slightly decrease the internal/local field and prevent the electronic leakage through the sample. Note that the conductivity exhibited a local maximum for each sample. For example, a peak was observed at 40 MV/m for the fresh film, whereas a peak was at 80 MV/m for the 200 MV/m-poled film. The reason could be attributed to the polarization of impurity ions in the sample, and this will be discussed in the TSDC study later.

Next, we investigated the effect of polarization of amorphous dipole on the electronic conduction in the BOPVDF film. To achieve aligned amorphous dipoles, we in situ polarized[51] the BOPVDF sample at a preset electric field below the E_c (i.e., 20 and 30 MV/m) at room temperature for 20 min. In this way, polarization of the β crystalline dipoles could be avoided. Without removing the poling electric field, the sample was cooled below its T_g (i.e., −80 °C) to freeze the aligned amorphous dipoles. The leakage current results for the BOPVDF film at −80 °C are shown in Figure 3C. Compared with the fresh film, the in situ polarized samples with oriented amorphous dipoles showed a lower conductivity, and the higher the in situ poling field the lower the conductivity at −80 °C when the applied field was above 50 MV/m. This result indicated that aligned amorphous dipoles could also decrease the local electric field and thus reduced the electronic conduction in the BOPVDF film. Meanwhile, the electronic conductivity for the 200 MV/m-poled film with aligned β dipoles was also measured at −80 °C. The values nearly overlapped with those for the fresh film under all tested electric fields. This result suggested that oriented β crystalline dipoles

DOI: 10.1021/acsami.5b02944
ACS Appl. Mater. Interfaces 2015, 7, 19894−19905

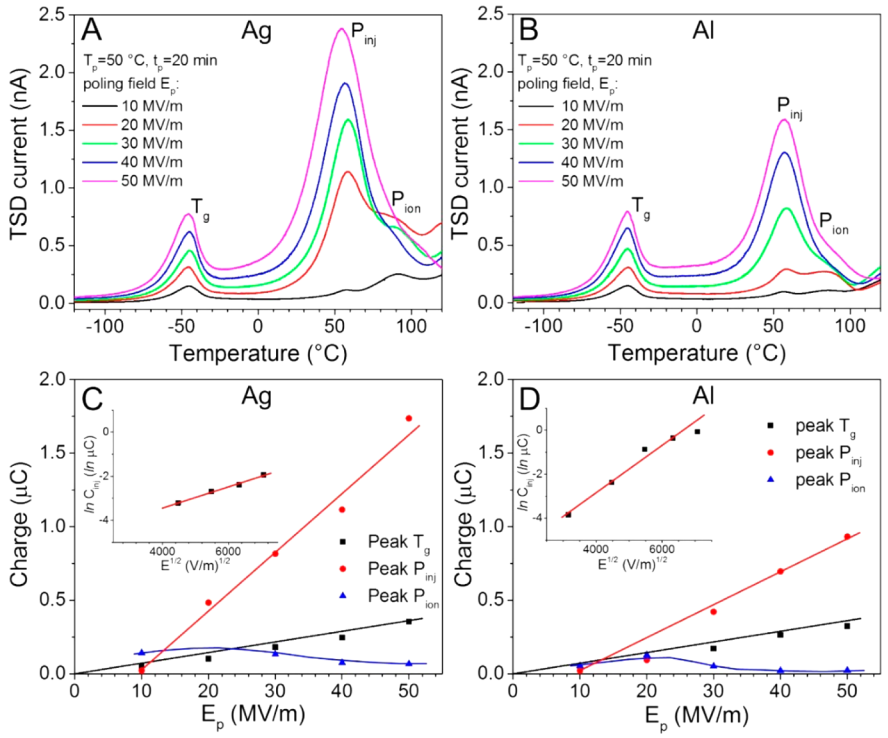

Figure 4. TSDC spectra for fresh BOPVDF films under different poling electric fields (E_p) at 50 °C for 20 min using (A) Ag and (B) Al electrodes. (C and D) Corresponding integration results for the three discharge peaks observed in the TSDC spectra in panels A and B. The peak-fitting results are shown in Figure S1 (Supporting Information).

were less effective in reducing the electronic conduction in the BOPVDF film than aligned amorphous dipoles. This is understandable because the conduction electrons must mostly pass through the amorphous phase rather than the PVDF crystals for insulating polymeric materials.

In addition to crystalline and amorphous dipoles, the electronic conductivity can also be affected by injected space charges (i.e., homocharges) and the impurity ions (i.e., heterocharges; Scheme 1). Here, we use the TSDC technique[34] to investigate both types of charges. In a TSDC experiment, three parameters, E_p, T_p, and t_p, are important for the subsequent discharge current spectrum. We will discuss the effects from these parameters in the following. Figure 4A shows the effect of the E_p on the TSDC spectra for fresh BOPVDF films polarized at 50 °C for 20 min with Ag electrodes. Three major discharge processes were observed around −45, 60 (slightly higher than the T_p of 50 °C), and 90 °C, respectively. To understand the nature of these discharge processes, each TSDC spectrum was deconvoluted into three peaks using peak-fitting software. The corresponding results are shown in Figures S1A−D (Supporting Information), where solid lines are the experimental data, and dotted lines are fitted peaks using the Lorentz function. From the fitted peaks, we obtained the charges (C) for three discharge process by integration in different temperature ranges: (1) −120 to −20 °C, (2) −20 to 120 °C, and (3) 50 to 120 °C. Figure 4C summarizes the discharged charges as a function of E_p during the three discharge events for the sample with Ag electrodes. First, the discharge peak at −45 °C could be attributed to the depolarization of the polarized amorphous PVDF via devitrification at T_g. Assuming the discharged charges at T_g (C_{Tg}) equal the dipolar polarization at 50 °C during the poling process in TSDC, the total charge density for the film at 50 °C, $D_{film}^{50°C}$, should be the summation of contributions from deformational ($D_{def,film}^{50°C}$) and dipolar ($D_{dip,film}^{50°C}$) electric displacements: $D_{film}^{50°C} = D_{def,film}^{50°C} + D_{dip,film}^{50°C}$, we obtain

$$\varepsilon_{rs,film}^{50°C}\varepsilon_0 E_p = \varepsilon_{r\infty,film}^{50°C}\varepsilon_0 E_p + C_{Tg}/A_0 \quad (4)$$

where $\varepsilon_{r\infty,film}^{50°C}$ and $\varepsilon_{rs,film}^{50°C}$ are the relative permittivity values of the BOPVDF film at high and low frequencies at 50 °C, and A_0 is the electrode area (0.786 cm^2). From Figure 2E, we can get $\varepsilon_{rs,film}^{50°C}$ = 12.7 at 0.1 Hz. Assuming $\varepsilon_{r\infty,film}^{50°C}$ is still 2.35 (namely, $\varepsilon_{r\infty,film}$ should not change much with temperature), a linear relationship can be obtained for the C_{Tg} as a function of the E_p; see the black line in Figure 4C. As we can see, the experimental data fit the theoretical line fairly well. The discharge peak at ca. 60 °C increased nearly linearly with E_p above 10 MV/m (see Figure 4A,C). We consider that this discharge peak should be related to the depolarization of the injected homocharges from Ag electrodes (P_{inj}, i.e., Schottky or thermionic emission[20,52]). To prove this hypothesis, we changed the electrodes from Ag to Al, because different metals should have different work functions and thus different charge injection capability.[34] Here, we choose Al instead of Au, because Al is much cheaper and is actually used as metal electrodes for nearly all polymer film capacitors.[1,2] The E_p-dependent TSDC spectra for Al electrodes are shown in Figure 4B, and the corresponding peak deconvolution results are shown in Figures S1E−H in the Supporting Information. Comparing the total charges (C_{inj}) for the P_{inj} peaks (Figure 4B,D), the C_{inj} for Ag electrodes was higher than that for Al electrodes. In addition, for Schottky emission at a constant temperature, the current density (J) scales as $\ln J \propto E_p^{1/2}$.[20,52] Assuming in a steady state, the injected charges equal the leakage charges and thus $C_{inj}/A_0 = \int$

DOI: 10.1021/acsami.5b02944
ACS Appl. Mater. Interfaces 2015, 7, 19894−19905

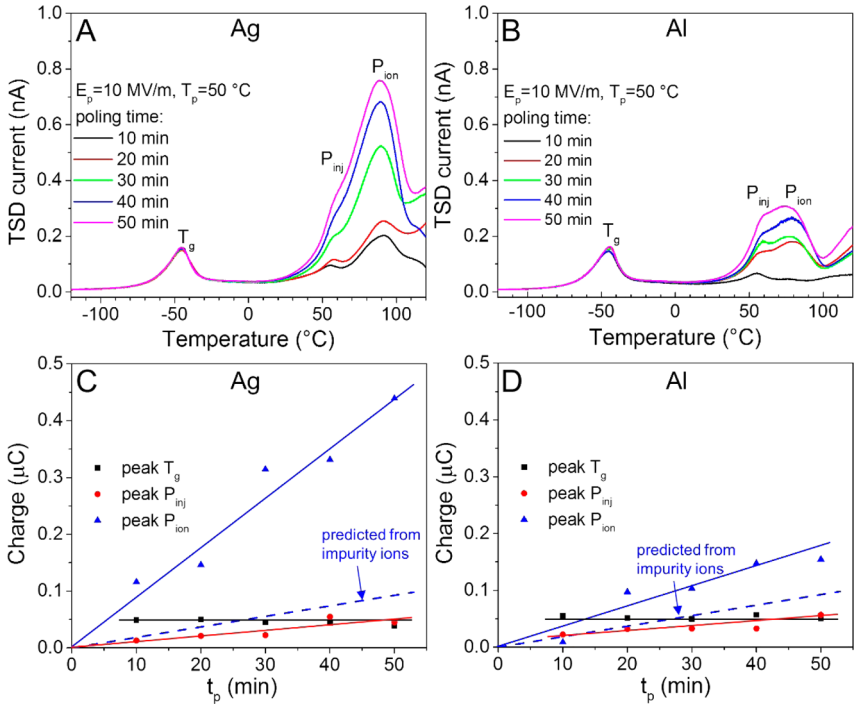

Figure 5. TSDC spectra for fresh PVDF films at different poling times (t_p) at 50 °C and 10 MV/m using (A) Ag and (B) Al electrodes. (C and D) Corresponding integration results for the three discharge peaks observed in the TSDC spectra in panels A and B. The peak-fitting results are shown in Figure S2 (Supporting Information).

J dt. As a result, the total charge should scale as ln $C_{inj} \propto E_p^{1/2}$. Indeed, the insets of Figure 4C,D showed a linear relationship between ln C_{inj} and $E_p^{1/2}$ for both Ag and Al electrodes. This was consistent with the above theoretical prediction. Both these result suggested that the discharge peak at ca. 60 °C could be assigned as the depolarization of the injected homocharges at 50 °C for 20 min. It is interesting to note that the charge injection only became important above 10 MV/m for both Ag and Al electrodes. Actually, in many practical applications the electric fields are above 10 MV/m; therefore, injected homocharges should always happen for real applications. From a previous report,[53] the injected homocharges were mostly positive charge carriers (holes) from the anode (positive electrode) into the vicinity of the sample−electrode interface. Upon subsequent heating, these charge carriers would discharge in a short-circuit TSDC run. For the sample with Al electrodes (Figure 4D), the discharged charge at T_g also fit to a linear relationship predicted by eq 4. Finally, the discharge peaks around 90 °C for samples with Ag and Al electrodes were often interfered by the premelting process of the poor PVDF secondary crystals (see DSC results in Figure 1C), which showed an up-turn in the discharge currents above 110 °C in Figure 4A,B. As a result, we could not conclude a well-defined trend for the charges from this discharge process if only based on the results in Figure 4.

To understand the origin of the discharge peak at 90 °C, TSDC experiments were carried out under 10 MV/m at 50 °C for different t_p values. An E_p of 10 MV/m, instead of 20 MV/m, was chosen because the interference from homocharge injection (i.e., the P_{inj} peak) could be minimized. TSDC spectra at different t_p values for the BOPVDF films with Ag and Al electrodes are shown in Figure 5A,B. Again, three discharge peaks in the TSDC spectra were deconvoluted using the Lorentz function (Figure S2, Supporting Information). The integration results of the discharge processes (i.e., charges) for films with Ag and Al electrodes are summarized in Figure 5C,D. From Figure 5A,B, the discharge peak position and area at the T_g remained constant regardless of different t_p values and different metal electrodes. This is understandable because the polarization of amorphous PVDF dipoles had a fast dynamics at 50 °C (<1 μs; see BDS results in Figure 2E,F). The P_{inj} peaks for BOPVDF samples with Ag and Al electrodes appeared around 60 °C (Figures 5A,B). The charges for the P_{inj} peaks only slightly increased with increasing the t_p (Figure 5C,D).

On the contrary, the discharge peak at 90 °C became significant and increased roughly linearly with the t_p for both samples with Ag and Al electrodes (Figures 5C and D). Given the slow dynamics, we consider that the discharge peak at 90 °C (P_{ion}) should be attributed to the depolarization of the polarized ions in the sample. If this was the case, the P_{ion} peak should be the same for the BOPVDF films despite the usage of different metal electrodes. Surprisingly, the P_{ion} peaks for the sample with Ag electrodes were apparently higher than that for the sample with Al electrodes (Figure 5C,D). We explain this observation as the following. Let us assume that both cations and anions in the BOPVDF film have a concentration of n_0 and their diffusion coefficients at 50 °C are the same, D_0. Assuming both cations and anions are single valence, the n_0 and D_0 values for the impurity ions at 50 °C can be extracted from the frequency scan BDS results in Figure 2E,F by fitting with the Sawada equations (fitting curves not shown):[21,22] $2n_0 = 5.606 \times 10^{18}$ ions/m^3 and $D_0 = 1.219 \times 10^{-15}$ m^2/s (note that in the Sawada fitting, the concentration is the summation of both cations and anions; therefore, the total concentration of ions is $2n_0$ if the concentrations for cations and anions are assumed to be same, n_0). Assuming the depolarization charges for ions (C_{ion}) is the same as the polarization of ions during the TSDC poling at 50 °C, the current density (J_{ion}) during the TSDC

DOI: 10.1021/acsami.5b02944
ACS Appl. Mater. Interfaces 2015, 7, 19894−19905

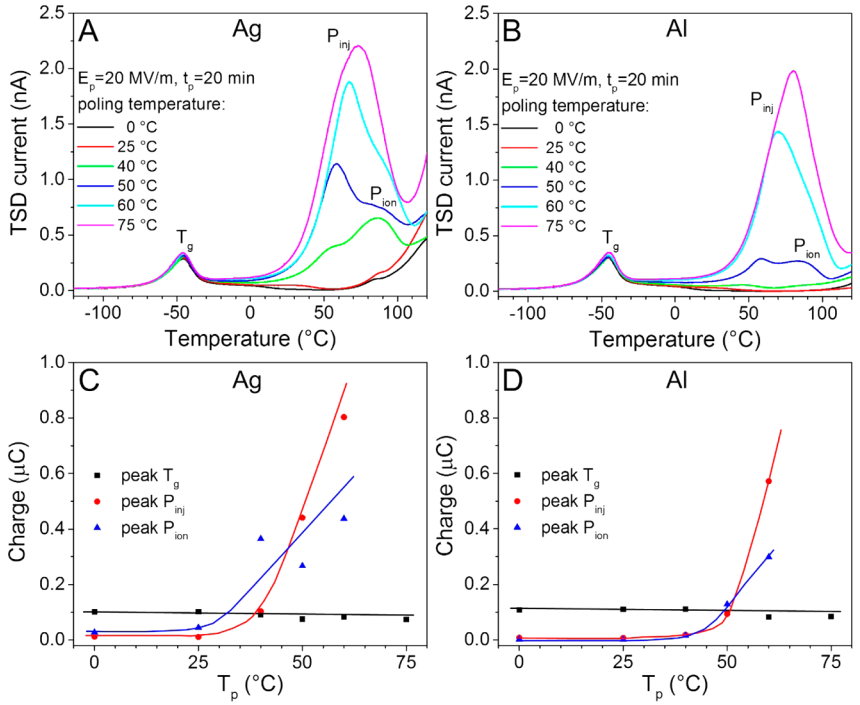

Figure 6. TSDC spectra for fresh BOPVDF films at different poling temperatures (T_ps) under 20 MV/m for 20 min using (A) Ag and (B) Al electrodes. (C and D) Corresponding integration results for the three discharge peaks observed in the TSDC spectra in panels A and B. The peak-fitting results are shown in Figure S3 (Supporting Information).

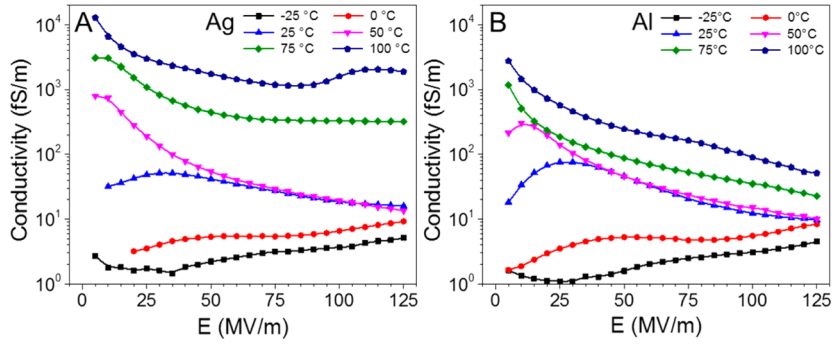

Figure 7. Conductivity as a function of electric field for fresh BOPVDF films with (A) Ag and (B) Al electrodes at different temperatures.

poling should be $J_{ion} = C_{ion}/(A_0 t_p)$. On the basis of a theoretical derivation for the total ionic current density from drifts of both cations and anions with the same D_0 under a constant poling electric field (E_p = 10 MV/m),[22] the J_{ion} can be expressed as

$$J_{ion} = \frac{C_{ion}}{A_0 t_p} = 2q^2 D_0 n_0 E_p / kT \quad (5)$$

If we assume only the impurity cations and anions in the BOPVDF film drift under E_p, the predicted relationship between C_{ion} and t_p are shown as the blue dashed lines in Figure 5C,D. Intriguingly, the experimental C_{ion} values for the P_{ion} peaks around 90 °C for both samples with Ag and Al electrodes appeared to be higher than the theoretical prediction. Considering that the experimental C_{ion} were different for different metal electrodes, there must be some electrochemical reactions between PVDF and the metal electrodes, which produce additional ionic species during electric poling at high fields and/or high temperatures. It is reported that PVDF tended to emit a certain amount of HF gas under high electric fields.[54] We speculate that Ag and Al must react with the emitted HF to produce Ag^+ and Al^{3+}, as well as F^- anions. Meanwhile, Ag appears to be more reactive with HF than Al, which is why the P_{ion} peaks for Ag are larger. Actually, we can see Ag electrode corrosion with naked eyes, especially on the positive (high voltage) side electrode after the BOPVDF film is polarized at high temperature (>100 °C), high electric field (>80 MV/m), and for a long time. We will discuss this in the leakage current study later.

To further prove the origin of P_{ion} peak from electrochemical reactions, we carried out a TSDC study for the BOPVDF film coated with Au electrodes. Results and discussion are included in section 6 in the Supporting Information. It is seen that the P_{ion} peak became fairly weak or nearly disappeared when Au electrodes were used for poling at E_p = 20 MV/m, T_p = 50 °C, and t_p = 20 min. This could be attributed to the higher electrochemical stability of Au than Ag and Al.

Finally, the effect of T_p on the TSDC spectra of the BOPVDF film was studied when the E_p was 20 MV/m and the t_p was 20 min. The corresponding results for samples with Ag and Al electrodes are shown in Figure 6A,B. The T_p range was

DOI: 10.1021/acsami.5b02944
ACS Appl. Mater. Interfaces 2015, 7, 19894−19905

from 0 to 75 °C. Again, three discharge peaks in the TSDC spectra in Figure 6A,B were fitted by the Lorentz function (Figure S3, Supporting Information). The integrated areas (i.e., charges) for samples with Ag and Al electrodes are summarized in Figure 6C,D. For the discharge peak at the T_g, the C_{Tg} remained nearly constant with T_p. The position for the P_{inj} peaks varied with the T_p, but was always 5−10 °C higher than the T_p. Meanwhile, with increasing the T_p, C_{inj} started to substantially increase above 40−50 °C. For the P_{ion} peaks around 90 °C, the C_{ion} also started to significantly increase above 40−50 °C. At T_p = 75 °C, the P_{inj} and P_{ion} peaks merged together, making the peak deconvolution not possible. However, judging from the peak shape and peak-fitting results (Figure 6C,D), the C_{inj} appeared always higher than the C_{ion} above 50 °C for both samples with Ag and Al electrodes. This suggested that charge injection dominated when the poling temperature was above 50−60 °C for the BOPVDF film under high field poling.

From the above study, both crystalline and amorphous dipoles should have limited effects on the electronic conduction in the BOPVDF film. What are the effects of the injected homocharges and the ions (both impurity ions and those generated from electrochemical reactions)? To answer this question, the DC conductivity of the BOPVDF films under different poling fields at different temperatures were tested for samples with Ag and Al electrodes, and results are shown in Figures 7A and B, respectively. At low temperatures (−25 and 0 °C), the conductivity increased slightly upon increasing the electric field for both samples with both Ag and Al electrodes. This was consistent with the electron-hopping conduction mechanism that electronic conductivity should increase with increasing the applied field.[9] When the temperature increased to 25 and 50 °C, the conductivity first increased and then decreased above a certain field, e.g., 30 MV/m for 25 °C and 5−10 MV/m for 50 °C. This phenomenon was nearly the same for both samples with Ag and Al electrodes. This can be explained as the following. In this temperature range at low electric fields, charge injection is limited. Instead, the polarized ions dominated in the poling process. Above a certain poling field, the polarized ions generated a strong enough opposite internal electric field and eventually decreased the electronic conduction. Note that the DC conductivities at 25 and 50 °C almost overlapped when the electric field was above 75 MV/m, suggesting that the effect of polarized ions from electrochemical reaction dominated at higher fields and longer poling times. When the temperature increased to 75 and 100 °C, the DC conductivity further increased for both samples with Ag and Al electrodes as compared to the conductivity at 50 °C. However, the increases were greater for the Ag than for the Al electrodes, which could be attributed to higher charge injection for the Ag electrodes at high temperatures under high electric fields. At each temperature, the conductivity still decreased with electric field, and this could be attributed to the polarized ions. For the BOPVDF film with Ag electrodes at 100 °C, an abnormal increase in conductivity was observed around 85 MV/m (Figure 7A). After the leakage current run at 100 °C, the sample was examined by naked eyes. The Ag electrode on the positive (high voltage) side lost its shiny metallic surface and also became not conductive, whereas the negative side still looked shiny and remained conductive. This proved our previous hypothesis that Ag electrode reacted with PVDF (most likely a small amount of HF gas) under high-field and high-temperature electric poling. This severe electrode corrosion could not be observed by naked eyes when Al was used as electrodes, suggesting that Al was more resistive than Ag for the electrochemical reaction.

From this study, we learn that PVDF (or its copolymers) coated with non-noble metal electrodes (e.g., Ag and Al), cannot be used for film capacitor applications under stringent electrical conditions, such as high electric fields, long poling times, and high temperatures, because it will emit HF gas, which in turn corrodes the metal electrodes. Considering Au is too expensive to be used as metal electrodes for practical applications, we propose to end-cap PVDF with a dielectric polymer (e.g., polycarbonate, PC) in a sandwich geometry or in multilayer films[13,55] to prevent direct contact of PVDF with metal electrodes. This research currently is under investigation and will be reported in the future.

3. CONCLUSIONS

In summary, the crystalline structure−dielectric property relationship for a BOPVDF film with 54 wt % crystallinity were studied. The PVDF crystals contained about 70% α phase and 30% β phase. Through extraction of the static dielectric constant for the amorphous phase, a high value of ca. 21−22 at 25 °C was obtained, much higher than the values of 8−13 both experimentally measured and theoretically predicted using molecular dynamics simulation for amorphous PVDF.[39] Consequently, a model of a finite amorphous interphase having a homeotropic orientation with respect to the crystal basal plane was proposed. In other words, a significant amount of PVDF chains on the crystal basal plane adopted the switchboard, rather than the adjacent reentry (or chain-folding), model. This interphase was similar to the rigid amorphous fraction observed for crystalline polymers.[47] Based on the Debye equation (eq S11, Supporting Information), the fraction of this oriented amorphous interphase was estimated to be 28% (i.e., 55% of the entire amorphous PVDF), similar to the rigid amorphous fraction (∼30%) in poly(ethylene terephthalate) (PET).[56] From frequency-scan BDS study (Figure 2F), the amorphous relaxation peak was broader and weaker at temperatures close to the T_g than at high temperatures, suggesting a slower segmental dynamics for the homeotropic interphase regions. In the future, we propose to use solid-state ^{19}F NMR to experimentally determine the existence of this interphase fraction in semicrystalline PVDF and its copolymers.

Electronic conduction in the BOPVDF film was investigated by a leakage current study, and various polarization mechanisms, including dipolar polarization, charge injection, and polarization of ions, were studied by TSDC spectroscopy. It was observed that dipolar polarization (i.e., polarization of crystalline and amorphous dipoles) could slightly decrease the electronic conduction; however, the effects were fairly limited. Instead, homocharge injection from metal electrodes, which tended to increase the electronic conduction, was proved by TSDC to be the most important factor at high temperatures (>40−50 °C) under high electric fields (>10 MV/m). Different metal electrodes exhibited different charge injection capability. For example, Al electrodes showed less charge injection into the BOPVDF film than Ag electrodes. As a consequence, the film coated with Al electrodes exhibited lower conductivity than that coated with Ag electrodes at high temperatures (>75 °C) and under high poling fields. In addition, high ionic polarization in the sample was observed by TSDC at long poling times and high poling temperatures. The polarized ions could produce a

DOI: 10.1021/acsami.5b02944
ACS Appl. Mater. Interfaces 2015, 7, 19894−19905

reverse internal field and thus reduce electronic conduction. However, the amount of ionic polarization was higher than what was expected from the impurity ions in the sample alone, suggesting that additional ions were generated from electrochemical reactions between PVDF and metal electrodes under harsh electrical poling conditions. Al electrodes appeared to be more resistant to the electrochemical reaction than Ag electrodes. To prevent direct electrochemical reactions between PVDF and the metal electrodes, we propose to carry out future research to sandwich PVDF with thin layers of a stable dielectric polymer such as PC (e.g., in multilayer films[13,55]).

■ ASSOCIATED CONTENT

Supporting Information

Experimental section, extraction of dielectric constant for the amorphous phase in BOPVDF, estimation of the fraction of oriented amorphous interphase in BOPVDF, derivation of dipolar polarizability in a 2D space, deconvolution results of TSDC spectra, and TSDC spectra with different metal electrodes. The Supporting Information is available free of charge on the ACS Publications website at DOI: 10.1021/acsami.5b02944.

■ AUTHOR INFORMATION

Corresponding Author

* E-mail: lxz121@case.edu. Tel. 01-216-3685861.

Notes

The authors declare no competing financial interest.

■ ACKNOWLEDGMENTS

This work was supported by Army Research Office (ARO) under award number W911NF-13-1-0153. The Novocontrol Concept 80 dielectric spectrometer was purchased under an award from the Defense University Research Instrumentation Program (DURIP), N00014-1-1-0805. The authors acknowledge Dr. Maya Endoh and Professor Tadanori Koga at University of Stony Brook for assistance with the synchrotron WAXD experiments. The synchrotron X-ray experiments were carried out at the National Synchrotron Light Source, Brookhaven National Laboratory, supported by the U.S. Department of Energy. Finally, the authors would thank Professor Peter Frübing at University of Potsdam, Germany, for helpful discussion on detailed TSDC measurements.

■ REFERENCES

(1) Sarjeant, W. J.; Zirnheld, J.; MacDougall, F. W. Capacitors. *IEEE Trans. Plasma Sci.* **1998**, *26*, 1368−1392.
(2) Sarjeant, W. J.; Clelland, I. W.; Price, R. A. Capacitive Components for Power Electronics. *Proc. IEEE* **2001**, *89*, 846−855.
(3) Montanari, D.; Saarinen, K.; Scagliarini, F.; Zeidler, D.; Niskala, M.; Nender, C. Film capacitors for automotive and industrial applications. In *Proceedings of CARTS U.S.A. 2009*; Jacksonville, FL, March 30−April 2, 2009.
(4) Husain, I. *Electric and Hybrid Vehicles: Design Fundamentals*; CRC Press: Boca Raton, FL, 2010.
(5) Barshaw, E. J.; White, J.; Chait, M. J.; Cornette, J. B.; Bustamante, J.; Folli, F.; Biltchick, D.; Borelli, G.; Picci, G.; Rabuffi, M. High Energy Density (HED) Biaxially-Oriented Poly-propylene (BOPP) Capacitors for Pulse Power Applications. *IEEE Trans. Magn.* **2007**, *43*, 223−225.
(6) Bluhm, H.; Rusch, D. *Pulsed Power Systems: Principles and Applications*; Springer: Berlin, 2006.
(7) Rasouli, M.; Phee, L. S. J. Energy Sources and Their Development for Application in Medical Devices. *Expert Rev. Med. Devices* **2010**, *7*, 693−709.
(8) Ho, J.; Jow, T. R. *Characterization of High Temperature Polymer Thin Films for Power Conditioning Capacitors*; Army Research Laboratory: Adelphi, MD, 2009.
(9) Ho, J.; Jow, T. R. High Field Conduction in Biaxially Oriented Polypropylene at Elevated Temperature. *IEEE Trans. Dielectr. Electr. Insul.* **2012**, *19*, 990−995.
(10) Nishino, A. Capacitors: Operating Principles, Current Market and Technical Trends. *J. Power Sources* **1996**, *60*, 137−147.
(11) Chu, B.; Zhou, X.; Ren, K.; Neese, B.; Lin, M. R.; Wang, Q.; Bauer, F.; Zhang, Q. M. A Dielectric Polymer with High Electric Energy Density and Fast Discharge Speed. *Science* **2006**, *313*, 334−336.
(12) Zhu, L.; Wang, Q. Novel Ferroelectric Polymers for High Energy Density and Low Loss Dielectrics. *Macromolecules* **2012**, *45*, 2937−2954.
(13) Zhu, L. Exploring Strategies for High Dielectric Constant and Low Loss Polymer Dielectrics. *J. Phys. Chem. Lett.* **2014**, *5*, 3677−3687.
(14) Yang, L.; Li, X.; Allahyarov, E.; Taylor, P. L.; Zhang, Q. M.; Zhu, L. Novel Polymer Ferroelectric Behavior via Crystal Isomorphism and the Nanoconfinement Effect. *Polymer* **2013**, *54*, 1709−1728.
(15) Jow, T. R.; Cygan, P. J. Dielectric Breakdown of Polyvinylidene Fluoride and its Comparisons with Other Polymers. *J. Appl. Phys.* **1993**, *73*, 5147−5151.
(16) Lovinger, A. J. Ferroelectric Polymers. *Science* **1983**, *220*, 1115−1121.
(17) Nalwa, H. S. *Ferroelectric Polymers: Chemistry, Physics, and Applications*; Marcel Dekker: New York, NY, 1995.
(18) Furukawa, T.; Nakajima, K.; Koizumi, T.; Date, M. Measurements of Nonlinear Dielectric in Ferroelectric Polymers. *Jpn. J. Appl. Phys.* **1987**, *26*, 1039−1045.
(19) Guan, F.; Wang, J.; Pan, J.; Wang, Q.; Zhu, L. Time and Poling History Dependent Energy Storage and Discharge Behaviors in Poly(vinylidene fluoride-*co*-hexafluoropropylene) Random Copolymers. *Chin. J. Polym. Sci.* **2011**, *29*, 65−80.
(20) Kao, K.-C. *Dielectric Phenomena in Solids: With Emphasis on Physical Concepts of Electronic Processes*; Elsevier Academic Press: Boston, MA, 2004.
(21) Mackey, M.; Schuele, D. E.; Zhu, L.; Baer, E. Layer Confinement Effect on Charge Migration in Polycarbonate/Poly(vinylidene fluorid-*co*-hexafluoropropylene) Multilayered Films. *J. Appl. Phys.* **2012**, *111*, 113702.
(22) Yang, L.; Allahyarov, E.; Guan, F.; Zhu, L. Crystal Orientation and Temperature Effects on Double Hysteresis Loop Behavior in a Poly(vinylidene fluoride-*co*-trifluoroethylene-*co*-chlorotrifluoroethylene)-*graft*-Polystyrene Graft Copolymer. *Macromolecules* **2013**, *46*, 9698−9711.
(23) Ameduri, B. From Vinylidene Fluoride (VDF) to the Applications of VDF-Containing Polymers and Copolymers: Recent Developments and Future Trends. *Chem. Rev.* **2009**, *109*, 6632−6686.
(24) Kim, S. H.; Hong, K.; Xie, W.; Lee, K. H.; Zhang, S. P.; Lodge, T. P.; Frisbie, C. D. Electrolyte-Gated Transistors for Organic and Printed Electronics. *Adv. Mater.* **2013**, *25*, 1822−1846.
(25) Tashiro, K., Crystal Structure and Phase Transition of PVDF and Related Copolymers. In *Ferroelectric Polymers: Chemistry, Physics, and Applications*, Nalwa, H. S., Ed.; Marcel Dekker: New York, NY, 1995; Chapter 2, pp 63−182.
(26) Lovinger, A. J. Annealing of Poly(vinylidene fluoride) and Formation of a 5th Phase. *Macromolecules* **1982**, *15*, 40−44.
(27) Demeuse, M. T. *Biaxial Stretching of Film: Principles and Applications*; Woodhead Publishing: Oxford, 2011.
(28) Kobayashi, M.; Tashiro, K.; Tadokoro, H. Molecular Vibrations of Three Crystal Forms of Poly(vinylidene fluoride). *Macromolecules* **1975**, *8*, 158−171.
(29) Gregorio, J. R.; Cestari, M. Effect of Crystallization Temperature on the Crystalline Phase Content and Morphology of Poly(vinylidene fluoride). *J. Polym. Sci., Part B: Polym. Phys.* **1994**, *32*, 859−870.
(30) Zhong, G.; Zhang, L.; Su, R.; Wang, K.; Fong, H.; Zhu, L. Understanding Polymorphism Formation in Electrospun Fibers of

DOI: 10.1021/acsami.5b02944
ACS Appl. Mater. Interfaces 2015, 7, 19894−19905

Immiscible Poly(vinylidene fluoride) Blends. *Polymer* **2011**, *52*, 2228−2237.
(31) Womes, M.; Bihler, E.; Einsenmenger, W. Dynamics of Polarization Growth and Reversal in PVDF Films. *IEEE Trans. Electr. Insul.* **1989**, *24*, 461−468.
(32) Jones, J.; Zhu, L.; Tolk, N.; Mu, R. Investigation of Ferroelectric Properties and Structural Relaxation Dynamics of Polyvinylidene fluoride Thin Film via Second Harmonic Generation. *Appl. Phys. Lett.* **2013**, *103*, 072901.
(33) Giacometti, J. A.; Ribeiro, P. A.; Raposo, M.; Maratmendes, J. N.; Campos, J. S. C.; Dereggi, A. S. Study of Poling Behavior of Biaxially Stretched Poly(Vinylidene Fluoride) Films Using the Constant-Current Corona Triode. *J. Appl. Phys.* **1995**, *78*, 5597−5603.
(34) Sessler, G. H.; Gerhard-Multhaupt, R. *Electrets*. 3rd ed.; Laplacian Press: Morgan Hill, CA, 1998.
(35) Wang, Z.-G.; Hsiao, B. S.; Sauer, B. B.; Kampert, W. G. The Nature of Secondary Crystallization in Poly(ethylene terephthalate). *Polymer* **1999**, *40*, 4615−4627.
(36) Pan, M.; Yang, L.; Wang, J.; Tang, S.; Zhong, G.; Su, R.; Sen, M. K.; Endoh, M. K.; Koga, T.; Zhu, L. Composite Poly(vinylidene fluoride)/Polystyrene Latex Particles for Confined Crystallization in 180 nm Nanospheres via Emulsifier-Free Batch Seeded Emulsion Polymerization. *Macromolecules* **2014**, *47*, 2632−2644.
(37) Zhong, G.; Su, R.; Zhang, L.; Wang, K.; Li, Z.; Fong, H.; Zhu, L. Evolution of Nanodroplets and Fractionated Crystallization in Thermally Annealed Electrospun Blend Fibers of Poly(vinylidene fluoride) and Polysulfone. *Polymer* **2012**, *53*, 4472−4480.
(38) Wunderlich, B. *Thermal Analysis of Polymeric Materials*; Springer: Berlin, 2005.
(39) Karasawa, N.; Goddard, W. A., III Force Fields, Structures, and Properties of Poly(vinylidene fluoride) Crystals. *Macromolecules* **1992**, *25*, 7268−7281.
(40) Hahn, B.; Wendorff, J.; Yoon, D. Y. Dielectric Relaxation of the Crystal-Amorphous Interphase in Poly(vinylidene fluoride) and its Blends with Poly(methyl methacrylate). *Macromolecules* **1985**, *18*, 718−721.
(41) Gregorio, R., Jr.; Ueno, E. M. Effect of Crystalline Phase, Orientation and Temperature on the Dielectric Properties of Poly(vinylidene fluoride) (PVDF). *J. Mater. Sci.* **1999**, *34*, 4489−4500.
(42) Guan, F.; Pan, J.; Wang, J.; Wang, Q.; Zhu, L. Crystal Orientation Effect on Electric Energy Storage in Poly(vinylidene fluoride-*co*-hexafluoropropylene) Copolymers. *Macromolecules* **2010**, *43*, 384−392.
(43) Mandelkern, L. The Structure of Crystalline Polymers. *Acc. Chem. Res.* **1990**, *23*, 380−386.
(44) Mijovic, J.; Sy, J. W.; Kwei, T. K. Reorientational Dynamics of Dipoles in Poly(vinylidene fluoride)/Poly(methyl methacrylate) (PVDF/PMMA) Blends by Dielectric Spectroscopy. *Macromolecules* **1997**, *30*, 3042−3050.
(45) Blythe, A. R.; Bloor, D. *Electrical Properties of Polymers*. 2nd ed.; Cambridge University Press: Cambridge, 2005.
(46) Tyagi, M.; Alegria, A.; Colmenero, J. Heterogeneous Dynamics of Poly(vinyl acetate) far above Tg: A Combined Study by Dielectric Spectroscopy and Quasielastic Neutron Scattering. *J. Chem. Phys.* **2005**, *122*, 244909.
(47) Wunderlich, B. Reversible Crystallization and the Rigid-Amorphous Phase in Semicrystalline Macromolecules. *Prog. Polym. Sci.* **2003**, *28*, 383−450.
(48) Kremer, F.; Schönhals, A. *Broadband Dielectric Spectroscopy*; Springer: Berlin, 2003.
(49) Yang, L. Y.; Tyburski, B. A.; Domingues Dos Santos, F.; Endoh, M. K.; Koga, T.; Huang, D.; Wang, Y. J.; Zhu, L. Relaxor Ferroelectric Behavior from Strong Physical Pinning in a Poly(vinylidene fluoride-*co*-trifluoroethylene-*co*-chlorotrifluoroethylene) Random Terpolymer. *Macromolecules* **2014**, *47*, 8119−8125.
(50) Tseng, J. K.; Tang, S.; Zhou, Z.; Mackey, M.; Carr, J. M.; Mu, R.; Flandin, L.; Schuele, D. E.; Baer, E.; Zhu, L. Interfacial Polarization and Layer Thickness Effect on Electrical Insulation in Multilayered Polysulfone/Poly(vinylidene fluoride) Films. *Polymer* **2014**, *55*, 8−14.
(51) Dhinojwala, A.; Wong, G. K.; Torkelson, J. M. Rotational Reorientation Dynamics of Disperse Red-1 in Polystyrene - α-Relaxation Dynamics Probed by 2nd-Harmonic Generation and Dielectric Relaxation. *J. Chem. Phys.* **1994**, *100*, 6046−6054.
(52) Chiu, F. C. A Review on Conduction Mechanisms in Dielectric Films. *Adv. Mater. Sci. Eng.* **2014**, *2014*, 1.
(53) Mizutani, T.; Nagata, T.; Ieda, M. TSC Due to Space Charge in Polyvinylidene Fluoride. *J. Phys. D: Appl. Phys.* **1984**, *17*, 1883−1887.
(54) Eberle, G.; Schmidt, H.; Eisenmenger, W. Influence of Poling Conditions on the Gas Emission of PVDF. *IEEE 1993 Annual Report* **1993**, 263−268.
(55) Mackey, M.; Schuele, D. E.; Zhu, L.; Flandin, L.; Wolak, M. A.; Shirk, J. S.; Hiltner, A.; Baer, E. Reduction of Dielectric Hysteresis in Multilayered Films via Nanoconfinement. *Macromolecules* **2012**, *45*, 1954−1962.
(56) Okazaki, I.; Wunderlich, B. Modulated Differential Scanning Calorimetry in the Glass Transition Region. 5. Activation Energies and Relaxation Times of Poly(ethylene terephthalate)s. *J. Polym. Sci., Part B: Polym. Phys.* **1996**, *34*, 2941−2952.

DOI: 10.1021/acsami.5b02944
ACS Appl. Mater. Interfaces 2015, 7, 19894−19905